Available online at www.sciencedirect.com
ScienceDirect
Journal of Power Sources 172 (2007) 962–969
JOURNAL OF POWER SOURCES
www.elsevier.com/locate/jpowsour

Discharge rate capabilities of alkaline $AgCuO_2$ electrode

Timothy W. Jones [a], Jenny S. Forrester [b], Alex Hamilton [a], Michael G. Rose [a], Scott W. Donne [a,*]

[a] *Discipline of Chemistry, Australia*
[b] *Discipline of Mechanical Engineering, The University of Newcastle, Callaghan, NSW 2308, Australia*

Received 5 March 2007; accepted 3 May 2007
Available online 21 May 2007

Abstract

A series of $AgCuO_2$ samples are prepared and tested as alkaline cathode materials for primary batteries. $AgCuO_2$ discharges via four equivalent-charge reduction processes, the rate capabilities of which are determined. At ambient temperature $AgCuO_2$ displays superior rate capabilities for the two highest voltage processes. For all samples, the rate capability of the two lower voltage processes is always superior to those at higher voltage. This is due to the electrode intrinsically doping itself with elemental silver during discharge as part of the second reduction process. The electrode compares favourably with commercial electrolytic manganese dioxide but is prone to self-discharge, the kinetics of which are also discussed.
© 2007 Elsevier B.V. All rights reserved.

Keywords: Silver cuprate; Alkaline cathode materials; Discharge rate capability; Battery; Self-discharge

1. Introduction

For portable electronic devices, batteries are the power source of choice. With such devices becoming lighter, more portable, and having more advanced technology incorporated into them, there is an increasing requirement for higher levels of power. This places an ever-increasing strain on the battery systems, which may not be able to power future devices. Thus, for advancements in electronic devices to continue, there must also be a parallel improvement in the performance of the battery systems.

Focusing on the electrode materials, battery performance may be enhanced either by improving existing systems through gaining a greater fundamental understanding of their characteristics, or by identifying and developing a 'next-generation' of battery material. The latter option is an attractive alternative as it may lead to a significant leap in battery performance.

To develop new cathode materials for primary batteries, one approach in identifying suitable candidates is to prepare metal oxides in which the metal has a higher-than-usual oxidation state. From a performance perspective, this desirably increases both the intrinsic potential and the capacity of the electrode. Examples of metal oxides synthesized using this scheme include $BaFeO_4$ ('super iron')—Fe(VI) [1,2], and $ACuO_2$ (A = Li, Na, K)—Cu(III) [3,4]. In this study, focus is placed on the copper(III) oxide, silver cuprate ($Ag^{I}Cu^{III}O_2$), which has received attention as both an alkaline [5] and a non-aqueous [6] cathode material.

The first member of the ternary Ag–Cu–O system was disclosed by Gómez-Romero et al. [7], namely, the copper(II) oxide, $Ag_2Cu_2O_3$, which adopts the three-dimensional paramelaconite (Cu_4O_3 [8]) structure. The corresponding Cu(III) species, $AgCuO_2$ (or possibly $Ag_2Cu_2O_4$–$Ag^{I}Ag^{III}Cu_2{}^{II}O_4$ [9]) has been prepared via several synthetic routes, which include (i) the "chimie douce" wet-chemical oxidation with $K_2S_2O_8$ [10], (ii) electrochemical oxidation at a Pt anode [9], or (iii) the ozonisation [11] of aqueous suspensions of the $Ag_2Cu_2O_3$ precursor. Irrespective of the synthetic route, $AgCuO_2$ adopts the two-dimensional layered delafossite ($CuFeO_2$) structure [5,12,13] (Fig. 1).

In alkaline electrolyte, $AgCuO_2$ has been observed to discharge via four equivalent-charge reduction processes [5]. Due to the large separation of each reduction peak, it has been possible to isolate and identify the intermediates via *ex situ* X-ray diffraction (XRD), with the mechanism outlined as follows:

$$2AgCuO_2 + H_2O + 2e^- \rightarrow Ag_2Cu_2O_3 + 2OH^- \quad (1)$$

$$Ag_2Cu_2O_3 + H_2O + 2e^- \rightarrow 2Ag + 2CuO + 2OH^- \quad (2)$$

* Corresponding author. Tel.: +61 2 4921 5477; fax: +61 2 4921 5472.

0378-7753/$ – see front matter © 2007 Elsevier B.V. All rights reserved.
doi:10.1016/j.jpowsour.2007.05.032

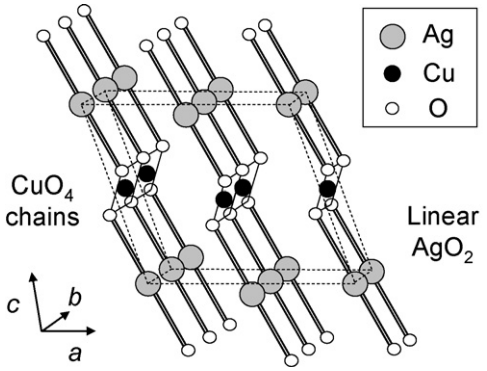

Fig. 1. Unit cell of $AgCuO_2$.

$$2CuO + H_2O + 2e^- \rightarrow Cu_2O + 2OH^- \quad (3)$$

$$Cu_2O + H_2O + 2e^- \rightarrow 2Cu + 2OH^- \quad (4)$$

Hence, the overall discharge process may be described as:

$$AgCuO_2 + 2H_2O + 4e^- \rightarrow Ag + Cu + 4OH^- \quad (5)$$

With novel electrode materials, certain aspects of their electrochemical performance may give the electrodes a niche market. One such aspect is the rate capability of the electrode. For instance, low rate capabilities may dictate that a material be used in an application where a slow, continuous discharge is desirable (*e.g.*, watches, hearing aids), whereas a system with a high rate capability may find an application where fast and frequent pulses of current are required (*e.g.*, camera flash batteries).

This paper reports an investigation of a series of $AgCuO_2$ samples as prospective alkaline cathode materials. Physical data (XRD, SEM and BET surface area) are related to the synthesis temperature and electrochemical performance, particularly the discharge rate capability. The rate capability is compared with that of electrolytic manganese dioxide (EMD), which is the current market leader in alkaline cathode materials.

2. Experimental

2.1. Material synthesis

A series of samples were prepared as a function of the synthesis temperature via the 'chimie douce' wet-chemical method outlined by Curda et al. [10]. A 1:1 stoichiometric solution of Ag^+/Cu^{2+} was prepared by dissolving 1.670 g $AgNO_3$ (9.83 mmol; UNIVAR) and 2.286 g $Cu(NO_3)_2{\cdot}2.5H_2O$ (9.83 mmol; UNIVAR) in 400 cm^3 of stirring de-ionised water. In a separate beaker, 7.6 g of NaOH (0.190 mol; Aldrich) was added to 100 cm^3 de-ionised water. These solutions were then mixed at the desired reaction temperature to initiate the co-precipitation reaction:

$$2Ag^+ + 2Cu^{2+} + 6OH^- \rightarrow Ag_2Cu_2O_3 + 3H_2O \quad (6)$$

This suspension was left stirring for 30 min after which 4.25 g of solid $Na_2S_2O_8$ (17.9 mmol; Aldrich) was added to oxidize the suspension:

$$Ag_2Cu_2O_3 + S_2O_8{}^{2-} + 2OH^- \rightarrow 2AgCuO_2 + 2SO_4{}^{2-} + H_2O \quad (7)$$

The suspension was allowed to oxidize for 1.5 h, followed by the addition of another 4.25 g of $Na_2S_2O_8$ and another 1.5 h oxidation period. The resulting solid was collected by vacuum filtration, and washed to neutrality with several 100 cm^3 volumes of water. Finally, the solid was dried in air at 70 °C overnight.

The commercial EMD sample was supplied by Delta EMD, Australia Pty Limited. It was prepared by the electrolysis of a hot (~95 °C), acidic solution of $MnSO_4$ ($[H_2SO_4]/[Mn^{2+}] = 0.3$), which resulted in the deposition of the EMD on to a titanium anode. Following deposition, the EMD was mechanically removed from the anode, milled to form a −105 μm powder, neutralized and washed to remove any entrained electrolyte, and then dried.

2.2. Physical characterization

2.2.1. X-ray diffraction (XRD)

A Phillips PW1710 diffractometer equipped with a Cu radiation source (Kα radiation, λ = 1.5418 Å) was used to obtain the powder X-ray diffraction pattern of each $AgCuO_2$ sample. Each diffraction pattern was recorded over the 2θ ranges of 10–90°, with a 0.04° step size and a 6 s count time.

2.2.2. Scanning electron microscopy (SEM)

Electron micrographs of the samples were obtained using a Phillips XL30 SEM at a variety of magnifications.

2.2.3. Gas adsorption/desorption

Surface areas of the samples were determined via a 9-point BET measurement, obtained with a Micromeritics ASAP 2020 Surface Area and Porosity Analyser in the partial pressure range 0.05–0.3 at 77 K.

2.3. Electrochemical characterization

All electrochemical tests were performed with a Princeton Applied Research VMP 16-channel potentiostat/galvanostat. The working electrode blackmix was prepared by mixing together active material ($AgCuO_2$ or EMD), SFG6 graphite and 9.0 M KOH in the mass ratio 0.1:1:0.2–0.3 with a mortar and pestle. The EMD blackmixes were allowed to equilibrate overnight, whereas those containing $AgCuO_2$ were tested immediately as they are known to be prone to self-discharge [14].

The electrochemical cell used has been described elsewhere [15]. Cell assembly involved placing the amount of blackmix corresponding to 15 mg of active material in a Teflon-lined C-size battery can. The sides of the Teflon sleeve were brushed down to remove attached particles and three separator papers were placed on top of the sample. A stainless-steel piston was then carefully inserted into the can and used to compress the blackmix (under 1 tonne) to form an electrode pellet within the cell. After compaction, the piston was removed from the cell and

replaced by a perforated Perspex separator disc and a cylindrical, stainless-steel, counter electrode. The chamber was filled with ~15 cm^3 of 9.0 M KOH electrolyte and a Perspex cap inserted. The cell was then mounted between the cover and base plate, on top of a brass current-collector, and held in place with three securing bolts that were each tightened to a torque of 75 cN m to ensure a uniform pressure. A Hg/HgO reference electrode was inserted to complete the cell. EMD tests were allowed an equilibration time (30 min) whilst $AgCuO_2$ electrodes were tested immediately.

Each sample was discharged galvanostatically at several rates in the range 10–250 mA g^{-1} and with linear sweep voltammetry (LSV) at 0.02 mV s^{-1}, from the open-circuit potential (OCP) to −0.9 V versus Hg/HgO.

3. Results and discussion

3.1. Physical characterization

3.1.1. Structural characterization

Powder X-ray diffraction patterns of the $AgCuO_2$ samples do not vary significantly as a function of synthesis temperature. The $AgCuO_2$ samples all have a two-dimensional layered delafossite structure (Fig. 1), as has been previously reported [13]. The Rietveld analysis of the powder XRD pattern is given in Fig. 2. $AgCuO_2$ crystallises in the *C*2/*m* space group, with the unit cell parameters $a_0 = 6.065$ Å, $b_0 = 2.807$ Å, $c_0 = 5.859$ Å and $\beta = 107.95°$, which are comparable with the original work [13].

3.1.2. Morphology

Scanning electron micrographs of the room temperature (22 °C) and 90 °C samples are presented in Fig. 3. The particle size is observed to decrease with increasing temperature. This is presumably due to nucleation being the favoured process compared with crystallite growth at higher temperatures.

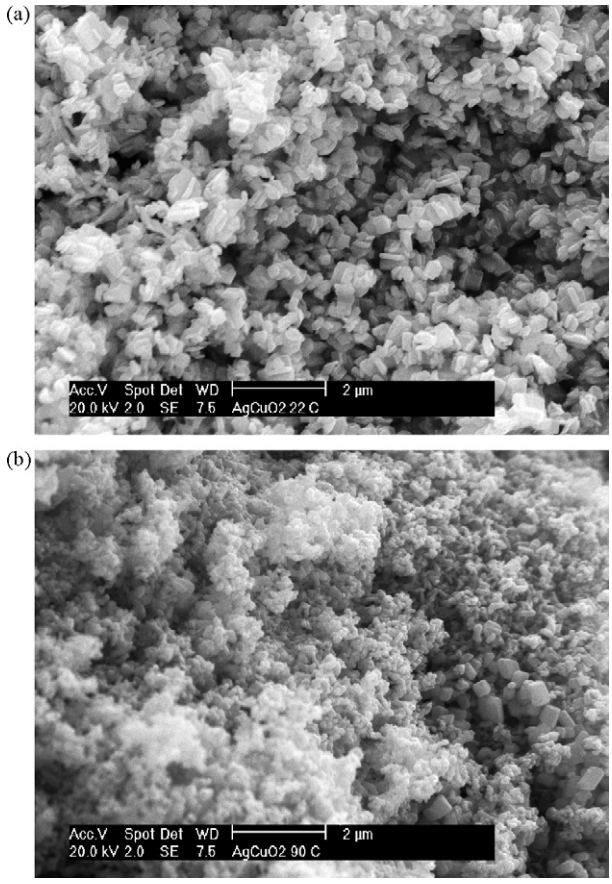

Fig. 3. Scanning electron micrographs of samples prepared at (a) 22 °C and (b) 90 °C.

3.1.3. Material BET surface area

The BET surface areas of the samples produced at different temperatures are shown in Fig. 4. All samples display relatively low surface areas (*i.e.*, <5 m^2 g^{-1}). Despite the grain size decreasing with increasing temperature, the material formed at

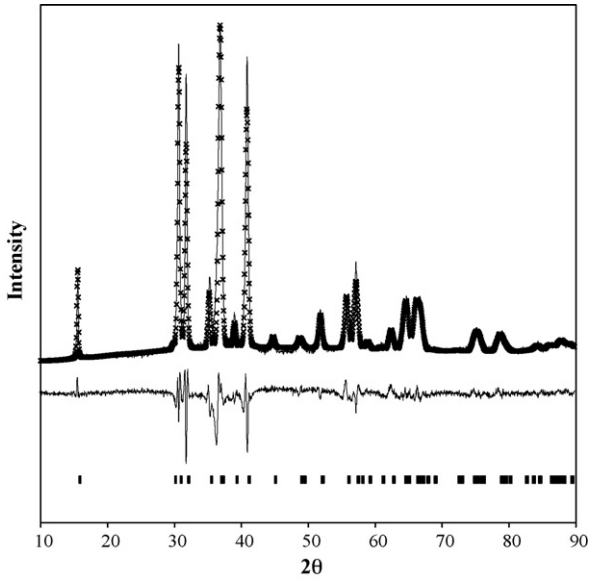

Fig. 2. Rietveld analysis of $AgCuO_2$.

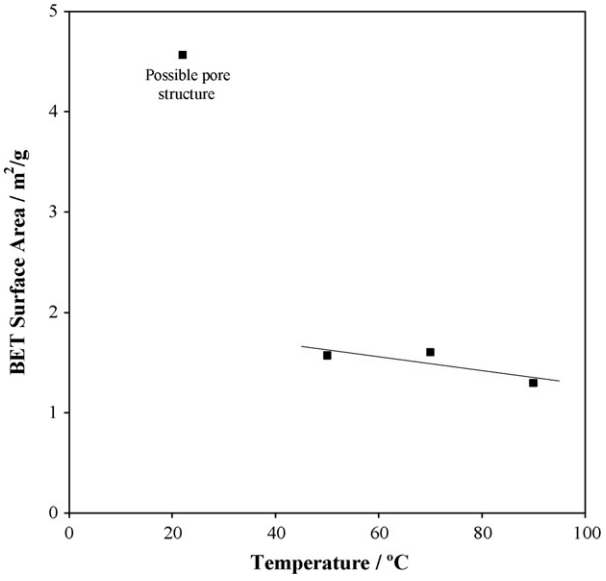

Fig. 4. BET surface areas of $AgCuO_2$ as function of synthesis temperature.

room temperature displays the highest surface area. This may be due to this sample having a more advanced pore structure than the other samples, which would have developed during crystallite growth. At lower temperatures, crystal growth is slower and more controlled, possibly allowing more advanced pore structures to develop, whereas at higher temperatures nucleation of new particles is favoured, and there is less time for such crystallite growth.

3.2. Electrochemical characterization

3.2.1. Voltammetry

The linear sweep voltammogram (LSV) of $AgCuO_2$ at $0.02\,mV\,s^{-1}$ is illustrated in Fig. 5(a). In alkaline electrolyte, $AgCuO_2$ is observed to discharge in four steps of approximately equivalent charge, as reported by Wang and co-workers [5].

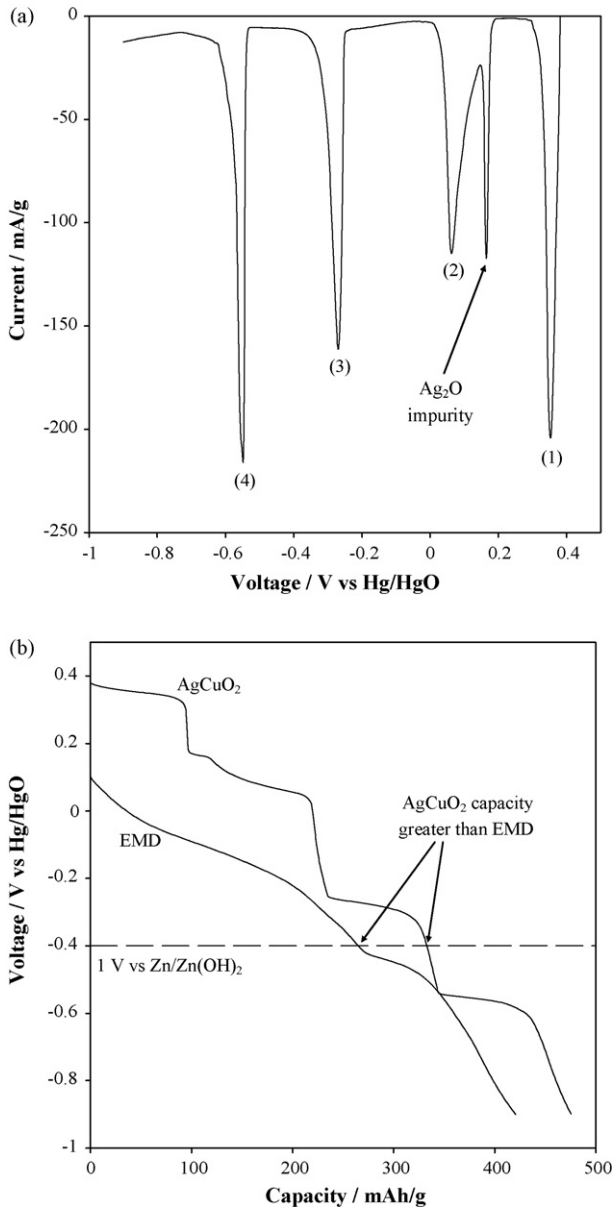

Fig. 5. (a) Linear sweep voltammogram of $AgCuO_2$ at $0.02\,mV\,s^{-1}$; (b) Discharge profile of $AgCuO_2$ compared with that of EMD.

The reduction processes ascribable to $AgCuO_2$ occur at +0.35, +0.04, −0.27 and −0.55 V versus Hg/HgO for processes (1)–(4), respectively. The synthesis impurity Ag_2O is observed as a low-capacity peak at +0.18 V, as was also reported by Wang and co-workers [5]. In both studies, however, Ag_2O is not found in the XRD pattern. The discharges profiles of $AgCuO_2$, and EMD are given in Fig. 5(b). Clearly, $AgCuO_2$ displays a considerably larger capacity than EMD; *i.e.*, 330 versus 260 mAh g^{-1}, respectively at −0.4 V. The capacity at this potential is chosen as it corresponds to roughly 1 V versus $Zn/Zn(OH)_2$, the anode material of choice in alkaline batteries, and also to the potential at which the discharge performance of EMD deteriorates [16]. $AgCuO_2$ is also a higher power electrode, with process (1) and (2) occurring at 0.31 and 0.21 V above that of EMD discharge at their respective capacities.

3.2.2. Rate capabilities

The rate capability of each discharge process was explored via the exchange current density (i_0) for each reduction. That is, the maximum galvanostatic discharge rate without significant deviation from the open-circuit potential (OCP) of the electrode for that process. Several phenomena during discharge may be rate-determining, and therefore dictate the magnitude of the exchange current density for each process. Each process may be limited by:

(i) access of electrolyte to the particle interior
(ii) a structural rearrangement of the material upon reduction
(iii) electron transport (conductivity) to the site of reduction.

Phenomenon (i) is a mass-transport limitation, whereas (ii) and (iii) are activation limitations. Trends in the exchange current densities of processes (1)–(4) for each sample in the series are illustrated in Fig. 6.

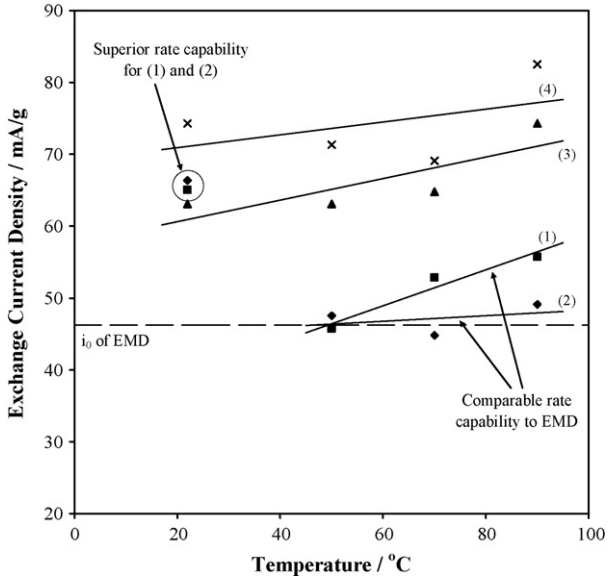

Fig. 6. Exchange current densities (i_0) of processes (1)–(4) for each sample of series.

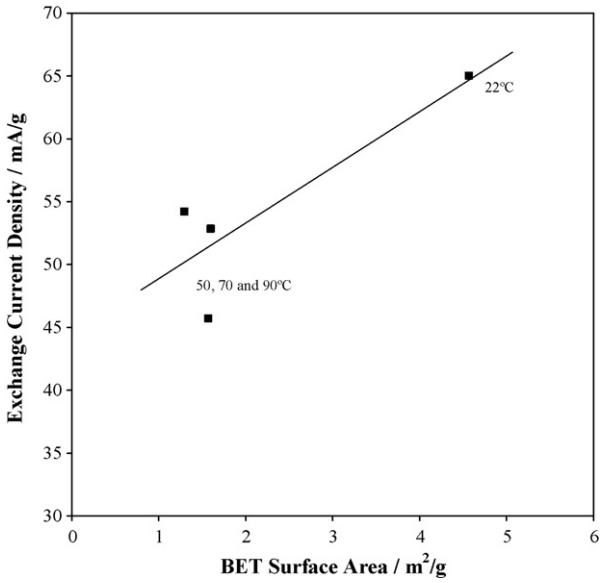

Fig. 7. Exchange current density of process (1) as function of BET surface area.

Firstly, consider processes (1) and (2). For samples prepared at elevated temperatures, the exchange current densities are comparable (within $\pm 5\,mA\,g^{-1}$) to one another and to that of EMD ($45–50\,mA\,g^{-1}$). There is, however, a notable increase of $\sim 15\,mA\,g^{-1}$ in i_0 for the sample produced at room temperature. Note that this sample also displayed the largest BET surface area (Fig. 4). The effect of BET surface area on the rate capabilities of process (1) is shown in Fig. 7. The exchange current density of process (1) increases with increasing BET surface area, which makes sense in terms of increasing the electrode|electrolyte interface. Nevertheless, the exchange current density only increases by 15%, compared with a 270% increase in BET surface area. Therefore, either the increase in i_0 is not solely due to an increased interfacial area and that another process becomes rate-determining, or that much of the increased surface area is in the form of pores that are difficult to access for the electrolyte, for instance narrow pore openings. The latter may be the case, as electrolyte penetration into pores would require time for equilibration, which was not allowed due to the tendency for process (1) to self-discharge at the OCP of the completed electrode. Overall, the rate capabilities of the four processes lie in the moderate discharge rate range, and typically increase from process (1)–(4). This is important because should an intermediate process display a significant drop in its rate capability, it could severely limit the performance of a battery in a moderate rate application after partial discharge.

Processes (3) and (4) have rate capabilities between 60 and $75\,mA\,g^{-1}$, which is $\sim 15\,mA\,g^{-1}$ higher than that of processes (1) and (2), with the exception of the 22 °C sample. These are roughly comparable for each respective process across the series (within $\pm 4\,mA\,g^{-1}$). Now, consider the reaction of process (2), where $Ag_2Cu_2O_3$ is reduced to CuO and Ag. That is, as the electrode discharges beyond process (2), it is effectively 'doping' itself at the micro-particulate level with elemental silver (an excellent conductor), as well as proceeding with mechanical degradation (increasing the electrode|electrolyte interface). These two phenomena are responsible for the observed increase in rate capabilities of processes (3) and (4) when compared with those of (1) and (2). The similarity of the exchange current densities may also imply some homogeneity at the micro-particulate level of the materials between the samples at this depth-of-discharge.

The idea of 'doping' a material at the micro-particulate level with a conductor has also been employed to increase the rate capability of materials with poor conductivity [17]. As a specific example, $LiFePO_4$ is seen as the long-term replacement of $LiCoO_2$ as a cathode material in non-aqueous Li-ion cells due to both its electrochemical performance in terms of excellent discharge potential, capacity and cyclablity, as well as socioeconomic factors such as it being environmentally benign and having a low cost compared with its would-be Li-ion predecessor [18]. The only aspect delaying its widespread commercial implementation is its low rate capabilities, due to a low specific conductivity ($\sim 10^{-9}\,S\,cm^{-1}$ [19]) owing to the material being ionic in nature. The conductivity has been improved by utilizing synthesis methods where the materials form composites with carbon (*i.e.,* $LiFePO_4$/C), which is comparable with our material 'doping' itself with silver (CuO/Ag composite) during discharge. An $LiFePO_4$/C composite prepared containing 12 wt.% internal carbon displayed markedly increased conductivities to the order of 10^{-2}–$10^{-3}\,S\,cm^{-1}$ [20].

3.2.3. Preliminary self-discharge investigation

The discharge profile for process (1) as a function of the galvanostatic discharge rate is given in Fig. 8. The inset displays the efficiency of process (1) as a function of the discharge rate. Reduction at higher discharge rates results in a greater efficiency of discharge. This is unusual as, typically, higher coulombic efficiencies are observed with lower discharge rates.

The above finding may be readily explained, however, by a self-discharge process. This is a competing reaction, and, is

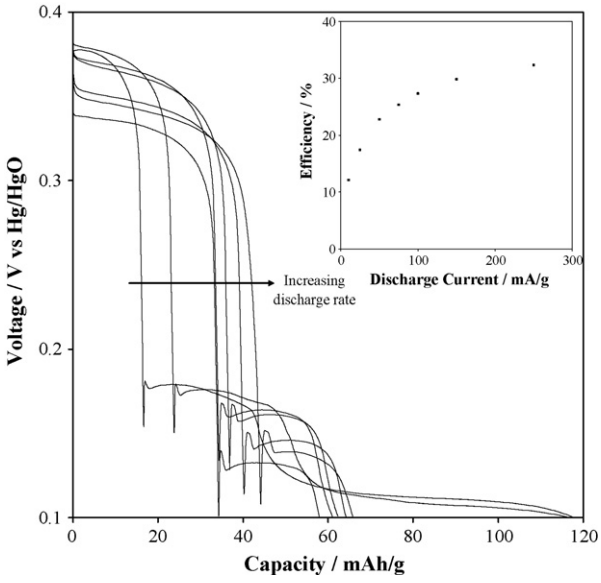

Fig. 8. Discharge profile of process (1) as function of galvanostatic discharge rate.

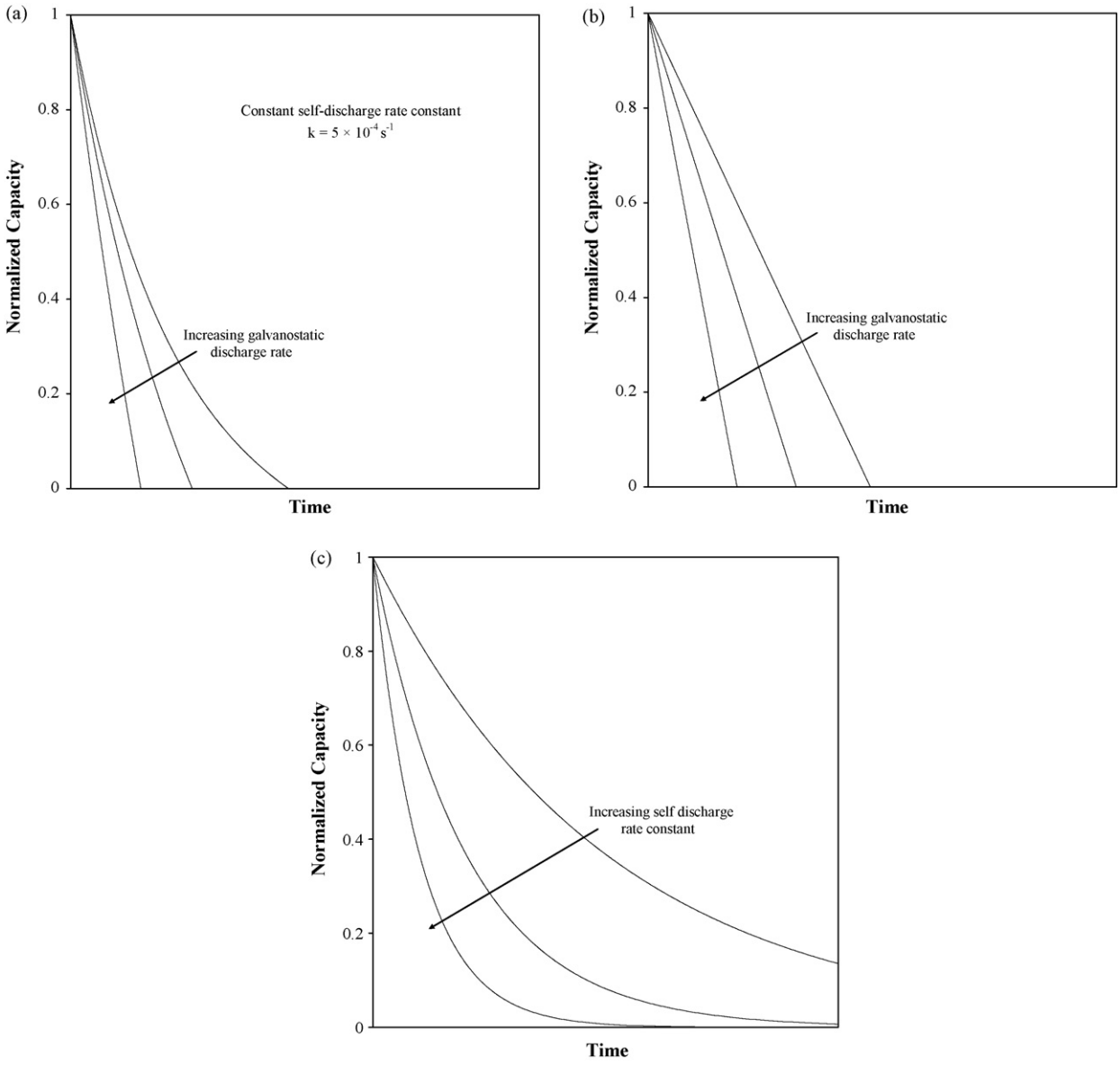

Fig. 9. Modelled examples of normalized capacity (Q_r/Q_0) as function of time for (a) purely first-order self-discharge, (b) purely galvanostatic discharge, and (c) total contribution of galvanostatic and self-discharge to overall extent of discharge.

likely to be due to catalytic oxygen evolution on graphite at the potential of the completed electrode [21], although oxidation of surface functional groups (*e.g.*, ≡C–OH, =C=O *etc*) has also been suggested [22]. Discharge at lower galvanostatic rates allows more time for the competitive self-discharge to take place, while discharge at higher rates gives less time for self-discharge. This is illustrated hypothetically in Fig. 9(a). First, if a first-order process is assumed for the electrode self-discharge via catalytic oxygen evolution on graphite, then the remaining capacity (Q_r) in the electrode is given by:

$$Q_r = Q_0 e^{-kt} + C \quad (8)$$

where $Q_0 + C$ is the initial capacity of the electrode; k is the first-order rate constant; t is the time; C is a constant that indicates the capacity remaining after self-discharge. Self-discharge is assumed to follow a first-order rate law strictly for the sake of simplicity, and fits well with the observed data. A calculated example of pure self-discharge is illustrated in Fig. 9(b). For purely galvanostatic discharge, the capacity decreases linearly from the theoretical capacity over time. This is illustrated in Fig. 9(c). The total capacity loss from galvanostatic and self-discharge will therefore resemble that of Fig. 9(a).

A first-order capacity decay model, in the form of Eq. (8), was used to determine the kinetic parameters (k, Q_0 and C) that relate to the self-discharge process. The parameters were fitted via linear least squares regression. The model was fitted successfully to experimental data, and selected examples are illustrated in Fig. 10. The important data from the kinetic model of self-discharge are listed in Table 1. The rate constant lie in the range $2.1–3.6 \times 10^{-4}\ s^{-1}$, which corresponds to capacity half-lives ($t_{1/2} = \ln 2/k$) of process (1) between 0.89

Table 1
Kinetic data determined from the model

Synthesis temperature T (°C)	First-order rate constant k ($\times 10^4$ s^{-1})	Capacity half-life $t_{1/2}$ (h)	Pre-exponential factor Q_0 (mAh g^{-1})	Constant C (mAh g^{-1})	Initial Capacity Q_i (mAh g^{-1})
90	3.45	0.56	39.89	10.39	50.28
70	2.97	0.65	46.49	16.39	62.88
50	3.60	0.53	54.04	8.13	62.16
22	2.16	0.89	61.51	5.88	67.39

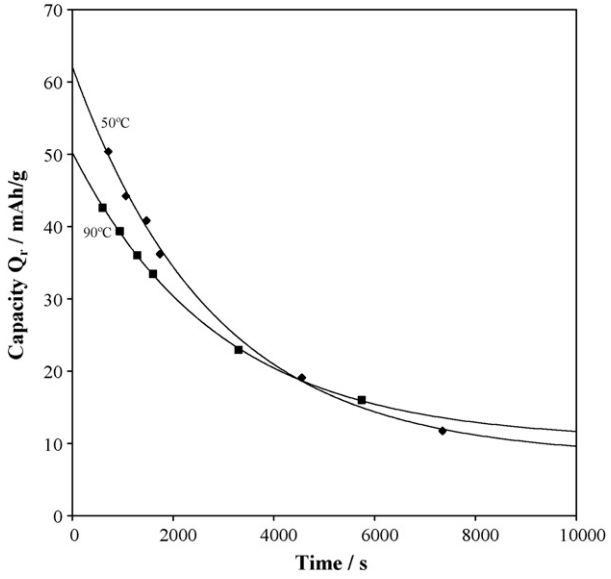

Fig. 10. Selected first-order self-discharge modeling (curved lines) from experimental data (symbols) for samples prepared at 90 and 50 °C.

and 0.53 h. As the electrode discharges, the concentration of Cu(III) in the electrode decreases, and the potential falls. Eventually, the potential will drop to a value at which self-discharge is either non-spontaneous or kinetically inhibited. The constant of integration (C) corresponds to the remaining capacity of the electrode at this potential.

In each case, the observed initial capacity ($Q_i = Q_0 + C$) is significantly less than the theoretical one-electron discharge for $AgCuO_2$ of 131.8 mAh g^{-1}. The duration of time from blackmix preparation (*i.e.*, the point at which self-discharge begins) through cell assembly, to the time of the commencement the electrochemical testing (*i.e.*, the observed initial capacity) is approximately 25 min. Therefore, the capacity of the electrode would have decayed significantly in this time. By way of example, the capacity of process (1) for the 50 °C sample is calculated to drop from 107.8 mAh g^{-1} (back-calculated initial capacity) to the observed 62.2 mAh g^{-1} during the estimated 25 min for assembly. That is, as the cell assembly time is comparable with the capacity half-life (32.1 min), and the capacity decreases to 57.7% of its original value.

4. Conclusions

$AgCuO_2$ is a high-power alkaline cathode material, which compares favourably with the current market leader in alkaline cathode materials, EMD, in terms of both average potential and useable capacity. It is also comparable in terms of its rate capabilities, where both materials are suitable for low–moderate rate applications. Nevertheless, the electrode suffers from an economic perspective, as the silver-containing material has a significantly higher manufacturing cost than EMD. This makes the alkaline $AgCuO_2$ electrode suitable only for niche applications, where large capacities are required. $AgCuO_2$ also suffers in terms of the self-discharge of process (1) in the completed electrode, which both decreases its capacity and the high starting potential that the first discharge process offers. Research on how to stabilize the electrode and stop or satisfactorily minimize the deleterious self-discharge process is required in order to increase the shelf-life and make use of its high capacity and potential. This is essential for the material to be incorporated into any commercial battery system.

Acknowledgements

The authors acknowledge financial support from the University of Newcastle and Delta EMD Australia Pty Limited, and are grateful to Jenny Zobec and Dave Phelan for their technical assistance.

References

[1] W. Yang, J. Wang, T. Pan, F. Cao, J. Zhang, C. Cao, Electrochim. Acta 49 (2004) 3455.
[2] K.A. Walz, A.N. Suyama, W.E. Sayama, J.J. Sene, W.A. Zeltner, E.M. Armacanqui, A.J. Roszkowski, M.A. Anderson, J. Power Sources 134 (2004) 318.
[3] H. Arai, S. Okada, Y. Sakurai, J. Yamaki, Solid State Ionics 106 (1998) 45.
[4] A.S. Prakash, D. Larcher, M. Morcette, M.S. Hegde, J.-B. Leriche, C. Masquelier, Chem. Mater. 17 (2005) 4406.
[5] C. Eylem, N. Iltchev, K. Nanjundaswamy, F. Wang, Electrochem. Solid State Lett. 7 (10) (2004) A346.
[6] C.D. May, J.T. Vaughey, Electrochem. Comm. 6 (2004) 1075.
[7] P. Gómez-Romero, E.M. Tejada-Rosales, M. Rosa Palaćin, Angew. Chem. 111 (1999) 544.
[8] P.E.D. Morgan, D.E. Partin, B.L. Chamberland, M. O'Keefe, J. Solid State Chem. 121 (1996) 33.
[9] D. Muñoz-Rojas, J. Oró, P. Gómez-Romero, J. Fraxedas, N. Casañ-Pastor, Electrochem. Comm. 4 (2002) 684.
[10] J. Curda, W. Klein, M. Jansen, J. Solid State Chem. 162 (2001) 220.
[11] D. Muñoz-Rojas, P. Gómez-Romero, J. Fraxedas, N. Casañ-Pastor, J. Solid State Chem. 178 (2005) 295.
[12] A.M. Sukeshini, H. Kobayashi, M. Tabuchi, H. Kageyama, Solid State Ionics 128 (2000) 33.
[13] J. Curda, W. Klein, H. Liu, M. Jansen, J. Alloys Compd. 338 (2002) 99.
[14] T.W. Jones, S.W. Donne, M.G. Rose, Unpublished Results.
[15] A.P. Malloy, G.J. Browning, S.W. Donne, J. Colloid Interface Sci. 285 (2) (2005) 653.
[16] K.E. Ayers, N.C. White, J. Electrochem. Soc. 152 (2005) A467.

[17] K.-F. Hsu, S.-Y. Tsay, B.-J. Hwang, J. Mater. Chem. 14 (17) (2004) 2690.
[18] A.K. Padhi, K.S. Nanjundaswamy, J.B. Goodenough, J. Electrochem. Soc. 144 (1997) 1188.
[19] S.J. Kwon, C.W. Kim, W.T. Jeong, K.S. Lee, J. Power Sources 137 (2004) 93.
[20] J. Lu, Z. Tang, Z. Zhang, W. Shen, J. Electrochem. Soc. 152 (2005) A1441.
[21] F. Bardé, M. Rosa Palaćin, B. Beaudoin, P.A. Christian, J.-M. Tarascon, J. Power Sources 160 (2006) 733.
[22] T. Arikardo, C. Iwakura, H. Yoneyama, H. Tamura, Electrochim. Acta 21 (1976) 551.